Journal Pre-proofs

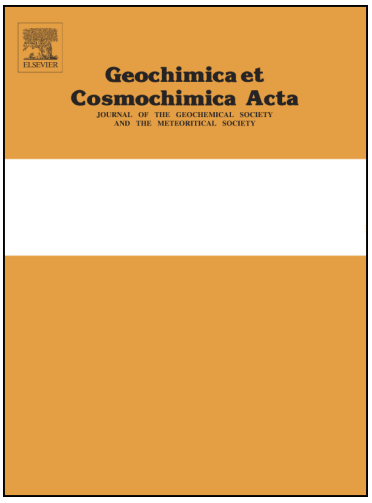

A model for germanium-silicon equilibrium fractionation in kaolinite

Alida Perez-Fodich, Louis A. Derry

PII: S0016-7037(20)30484-1
DOI: https://doi.org/10.1016/j.gca.2020.07.046
Reference: GCA 11872

To appear in: *Geochimica et Cosmochimica Acta*

Received Date: 20 March 2020
Accepted Date: 31 July 2020

Please cite this article as: Perez-Fodich, A., Derry, L.A., A model for germanium-silicon equilibrium fractionation in kaolinite, *Geochimica et Cosmochimica Acta* (2020), doi: https://doi.org/10.1016/j.gca.2020.07.046

A model for germanium-silicon equilibrium fractionation in kaolinite

Alida Perez-Fodich[a,b,c,*], Louis A. Derry[a,b]

[a] *Department of Earth and Atmospheric Sciences, Cornell University, Ithaca NY, USA*
[b] *Université de Paris, Institut de physique du globe de Paris, CNRS, F-75005 Paris, France*
[c] *Department of Geology, University of Chile, Santiago, Chile*

Abstract

Germanium is a useful tracer of silicate weathering and secondary mineral formation in the Critical Zone because Ge/Si ratios are fractionated during incongruent weathering of silicates. We develop an estimate of the equilibrium fractionation coefficient between germanium and silicon for the precipitation of kaolinite using a solid-solution model. Thermodynamic properties were estimated using observations from natural systems, experimental data from analog phyllo-germanate minerals (Shtenberg et al., 2017), and a parametric method based on a sum of oxides approach with site-specific interaction parameters (Blanc et al., 2015). The estimated $\log D'_{Ge-Si}$ for the incorporation of Ge into kaolinite at 25°C and 0.1 MPa is equal to –3.4 ± 1.5. The estimated ΔG_f° for a fully Ge substituted kaolinite ($Ge_2Al_2O_5(OH)_4$) equals –3130 ±15 (kJ/mol), and the estimated $\log(K_{sp})$ for Ge-kaolinite = 3.1 ± 1.5. We develop a series of batch reaction models using a geochemical reactive transport code to test the estimated range of the Ge-Si equilibrium fractionation coefficient. In these series of models, we also investigate how precipitation dynamics can impact the Ge/Si ratios observed both in streams and soils. These models show that both precipitation kinetics and re-equilibration of the precipitated solid control the behavior of Ge/Si ratios at far-from-equilibrium timescales. While the actual length of these timescales remains to be determined by better constraints on kaolinite precipitation rates at environmental conditions; our models suggest that the lowest groundwater measured Ge/Si ratios should represent this equilibrium timescale.

*Corresponding author
Email address: aliperez [at] uchile [dot] cl (Alida Perez-Fodich)

Keywords: , Silicon, Ge/Si, Weathering, Kaolinite, Equilibrium fractionation, Distribution coefficient, Critical Zone, Mineral Precipitation, Thermodynamic Data, Solubility

1. Introduction

The potential for the trace element germanium to substitute for silicon in silicate minerals and therefore provide insight into the behavior of silicate systems was recognized by Goldschmidt's seminal work (Goldschmidt, 1926). In natural waters unaffected by hydrothermal activity or coal ash contamination, germanium-silicon ratios (Ge/Si) are lower than in their source rocks, implying a fractionation of Ge from Si during the weathering process (Mortlock and Froelich, 1987). Observations from various systems indicate that igneous bedrocks have molar ratios of Ge/Si $\approx$ 1.5–2.5 $\times 10^{-6}$, while most streams and soil pore waters show $(Ge/Si)_{fluid} \approx$ 0.1–1 $\times 10^{-6}$. In some cases streams can reach higher values due to coal ash contamination (Froelich et al., 1985) or hydrothermal activity (Evans and Derry, 2002). The range in stream Ge/Si ratios has been explained in terms of weathering intensity W, the ratio of Si transported from the weathering system in the dissolved and solid phases (Murnane and Stallard, 1990). Based on this hypothesis, Froelich et al. (1992) derived an empirical partition coefficient $K_w = \frac{(Ge/Si)_{clay}}{(Ge/Si)_{bedrock}} \approx 2.5$ from the limited solid-phase data of Murnane and Stallard (1990), and showed that this was reasonably consistent with observations of a Ge-enriched soil and Ge-depleted stream water. The biological Si cycle can also influence the low Ge/Si ratios in river systems (Derry et al., 2005). However, the effect of the biogenic silica pool is typically limited by the contributions of shallow hydrologic pathways (Cornelis et al., 2010; Lugolobi et al., 2010; Ameijeiras-Marino et al., 2018).

Subsequent studies have extended these initial observations with increasing evidence that sequestration of Ge in secondary minerals is largely responsible for this fractionation, with clays enriched in Ge relative to coexisting solutions (Murnane and Stallard, 1990; Froelich et al., 1992; Kurtz et al., 2002; Lugolobi et al., 2010; Aguirre et al., 2017; Aguirre, 2019). For many igneous rocks, it can be argued that incongruent dissolution of feldspars to clays is the reaction most responsible for Ge-Si fractionation. The overall stoichiometry and mineralogy for this reaction will depend on the composition of the rock. A common example is the incongruent dissolution of plagioclase (in this case albite) to form kaolinite:

$$2\,\mathrm{NaAl(Si_{1-x}Ge_x)_3O_8} + 2\,\mathrm{H^+} + 9\,\mathrm{H_2O} = \\ \mathrm{(Si_{1-y}Ge_y)_2Al_2O_5(OH)_4} + 4z\mathrm{Ge(OH)_4} + 4(1-z)\mathrm{Si(OH)_4} + 2\,\mathrm{Na^+} \quad (1)$$

where, $x < y$ based on observed Ge/Si ratios in weathering systems (e.g. Froelich et al., 1992; Kurtz et al., 2002; Baronas et al., 2018), and $y = 3x - 2z$. A similar reaction can be written for the reaction of K-feldspar to illite, where the Si/Al ratio from the feldspar (≈ 3) changes to ≈ 1 in the clay—note that for different plagioclase compositions $1 \leq (Si/Al)_{plag} < 3$. Moreover, an analogue can be established for the non-crystalline phases dominating basaltic systems with dissolution of glass and plagioclase to precipitate allophane and imogolite (Wada and Wada, 1982; Kurtz et al., 2002). In granitoid weathering systems, $(Ge/Si)_{kaolinite}$ ratios are often ∼5–6 µmol/mol (Kurtz et al., 2002; Lugolobi et al., 2010; Aguirre et al., 2017; Aguirre, 2019) and for basaltic systems with poorly-crystalline secondary aluminosilicates $(Ge/Si)_{soil}$ ratios can reach > 10 µmol/mol (Kurtz et al., 2002; Qi et al., 2019). Because of the lack of thermodynamic constraints, despite the increasing evidence of Ge-Si partitioning into secondary clays, most of these studies continue to use the empirical derivation for the distribution coefficient K_w by Froelich et al. (1992). This empirically derived K_w represents a snapshot of the Ge-Si distribution in each system that can be obscured by different processes that occur during weathering, including biogenic Si cycling (Derry et al., 2005; Opfergelt et al., 2010) and adsorption onto Fe-oxyhydroxides (Anders et al., 2003; Scribner et al., 2006). Therefore, it is necessary to have a framework that can be used to reconcile the variance observed in Ge/Si ratios in soils, pore waters and rivers, as reaction (1) is of importance to understand the silicon global cycle. To date, there is only a limited dataset of thermodynamic properties for germanate minerals (Pokrovski and Schott, 1998; Shtenberg et al., 2017), and there is no thermodynamic data available for any type of aluminogermanate mineral.

Recent advances in models for estimating thermodynamic properties of clays can be applied to Ge-bearing clays (Blanc et al., 2015); while new developments in tracer–isotope tracking in reaction path and reactive transport codes permit testing the partitioning of germanium and silicon into clays and waters using the synthetic thermodynamic data (Druhan et al., 2013; Steefel et al., 2014). In this study, we calculate the equilibrium fractionation

coefficient for reaction (1) using an ideal solid-solution model based on available Ge/Si data and an independent method that predicts the thermodynamic properties of clays. To evaluate our results, we have developed a series of simulations designed to test these estimated solubility constants. The batch models treat Si and Ge-kaolinite as an ideal solid-solution; while tracking the partitioning of Ge and Si into the precipitated phase and the reacting fluid. These experiments allow us to test the effects of mineral precipitation equilibria and kinetics on the far-from-equilibrium behavior of Ge/Si ratios in both the fluid and mineral phases. We hypothesize that both the Ge-Si partitioning coefficient determined here and the overall precipitation rate of the newly formed Ge-Si kaolinite can explain much of the abiotic behavior of Ge-Si fractionation in soils and stream waters globally.

2. Calculation of thermodynamic properties of aluminogermanate clays

Assuming ideal substitution of Si by Ge in the tetrahedral site (Martin et al., 1992, 1996) the equilibrium fractionation of Ge/Si ratios during chemical weathering and precipitation of secondary minerals requires that the incorporation of Ge into the clay structure be much more thermodynamically favorable than Si. Germanium concentrations in rocks are typically 1–3 ppm and most natural waters range from 10 to 100 pmol/kg. Ge/Si ratios in rocks and minerals are between 0.5 to 5 µmol/mol; while most waters are 0.1–1 µmol/mol (Bernstein, 1985; Froelich et al., 1985; Kurtz et al., 2002; Evans and Derry, 2002). The six orders of magnitude difference between Ge and Si in most natural materials implies that the equilibrium concentration of $Ge(OH)_{4(aq)}$ for most phyllo-germanate phases should be much lower than for $Si(OH)_{4(aq)}$ for precipitation of analogous phyllosilicates (Prieto, 2009). To investigate equilibrium fractionation of Ge-Si during precipitation of secondary clays using geochemical reaction path and reactive transport codes, we need thermodynamic data for the formation and hydrolysis of an aluminogermanate phase. To our knowledge, thermodynamic data for Ge-bearing aluminosilicate clays have not been reported and data for only three synthetic phyllogermanates are available (Shtenberg et al., 2017). For our modeling purposes we have decided to calculate solubility coefficients for an aluminogermanate clay analog to kaolinite to investigate the partitioning of Ge and Si in weathering environments where precipitation of secondary clays—such as kaolinite—occurs. We have calculated the equilibrium constant for

the dissolution (or precipitation) of a completely Ge-substituted kaolinite $Ge_2Al_2O_5(OH)_4$—from now on "Ge-kaolinite"—based on two different methods: (1) using new Ge/Si data from springs and groundwaters (baseflow) in equilibrium with kaolinite (Aguirre, 2019) and Ge/Si ratios measured in kaolinite crystals (Kurtz et al., 2002; Lugolobi et al., 2010; Aguirre et al., 2017); and (2) we have also used an independent method to derive thermodynamic properties of clays—including ΔH_f°, S_f° and ΔG_f° (Blanc et al., 2015). We then compare both results with the only data available for phyllogermanates (Shtenberg et al., 2017).

2.1. Solid-solution model to estimate of the equilibrium fractionation of Ge and Si in kaolinite precipitation

For the equilibrium calculation the existence of an ideal solid solution between kaolinite and its Ge analogue is assumed. This relationship has been shown to exist in alkaline feldspar (Capobianco and Navrotsky, 1982), and has been assumed for other types of silicate minerals including wollastonite and quartz given the 6-orders of magnitude difference in Ge and Si concentration (Pokrovski and Schott, 1998; Evans and Derry, 2002). In the case of phyllosilicates, Martin et al. (1992, 1996) showed that Ge and Si atoms are randomly distributed in the tetrahedral sheet of synthetic talc. Thus, despite the differences in ionic radii between Si and Ge, it is safe to assume that non-ideal behavior in phyllosilicates is minimal. The hydrolysis reactions for both Ge and Si end-members are described as:

$$Ge_2Al_2O_5(OH)_4 + 6H^+ \longrightarrow 2Ge(OH)_{4(aq)} + 2Al^{3+} + H_2O_{(l)} \quad (2)$$

$$Si_2Al_2O_5(OH)_4 + 6H^+ \longrightarrow 2Si(OH)_{4(aq)} + 2Al^{3+} + H_2O_{(l)} \quad (3)$$

Using reactions (2) and (3) the equilibrium constant for the hydrolysis of Ge-kaolinite can be written in terms of the Ge/Si ratio in the fluid and the clay, plus the kaolinite equilibrium constant ${}^{Si}K_{sp}$ for reaction (3):

$${}^{Ge}K_{sp} = \frac{a^2_{Ge(OH)_4}}{a^2_{Si(OH)_4}} \times \frac{a_{Si-kaolinite}}{a_{Ge-kaolinite}} \times {}^{Si}K_{sp} \quad (4)$$

where, $a_{Ge(OH)_4}$ and $a_{Si(OH)_4}$ are the activity coefficients of germanic and silicic acids in aqueous solutions respectively, and $a_{Ge-kaolinite}$ and $a_{Si-kaolinite}$ are the activity coefficients

of $Ge_2Al_2O_5(OH)_4$ and $Si_2Al_2O_5(OH)_4$ in the mineral solid solution. Given the ideal solution behavior, the activities of each component in the mineral are represented by their mole fractions X_{Ge} and X_{Si}:

$$a_{Ge-kaolinite} = \left(X_{Ge}\right)^2 = \frac{(n_{Ge})^2}{(n_{Ge} + n_{Si})^2} \tag{5}$$

here n_{Ge} and n_{Si} are respectively the number of moles of Ge and Si in the clay. Therefore, the distribution coefficient (or equilibrium fractionation factor) D'_{Ge-Si} is given by:

$$\frac{^{Ge}K_{sp}}{^{Si}K_{sp}} = \frac{\left(Ge/Si\right)^2_{fluid}}{\left(Ge/Si\right)^2_{clay}} = D'_{Ge-Si} \tag{6}$$

note that we have defined the distribution coefficient D'_{Ge-Si} as the inverse of the squared partitioning coefficient, which would be: $K_D^2 = \frac{R_{solid}}{R_{fluid}} = \frac{1}{D'_{Ge-Si}}$ (where R represents the Ge/Si ratio). Also, the activity coefficients of germanic acid $Ge(OH)_4$ and silicic acids $Si(OH)_4$ are almost identical and that neither acid is significantly dissociated.

The equilibrium constant for the hydrolysis of kaolinite was obtained from the Thermoddem database (Blanc et al., 2012) (Table 3). We favor the use of this database because is internally consistent, and it is the most updated compilation of classical databases (e.g. Delany and Wolery, 1989) constructed from software packages (e.g. Johnson et al., 1992; Zimmer et al., 2016) and experimental data. We take the average Ge concentration in kaolinite to be 2.7 ppm ($n = 4$, Kurtz et al. (2002); Lugolobi et al. (2010)). Thus, in the ideal solid solution $Al_2(Si_{(1-x)}Ge_x)_2O_5(OH)_4$, the $(Ge/Si)_{clay} \approx 4.8$ µmol/mol. Ge/Si ratios from clean rivers range between $(Ge/Si)_{fluid} = 0.1$ to 1 µmol/mol (Froelich et al., 1985; Mortlock and Froelich, 1987; Murnane and Stallard, 1990; Froelich et al., 1992; Chillrud et al., 1994; Kurtz et al., 2002; Anders et al., 2003; Lugolobi et al., 2010; Aguirre et al., 2017; Ameijeiras-Marino et al., 2018). However, new data from groundwater and springs the Southern Sierra Critical Zone Observatory within the Kings River Experimental watershed (e.g. Bales et al., 2011; Liu et al., 2013) shows consistently lower Ge/Si ratios. The lowest Ge/Si ratios are recorded during the autumn and winter, when the streams are supplied only by groundwater (Liu et al., 2013; Hunsaker and Johnson, 2017). $(Ge/Si)_{fluid}$ ratios during baseflow discharge are < 0.1 µmol/mol, plus these waters are in equilibrium with kaolinite (Aguirre, 2019). This

baseflow component has been interpreted to have long residence times based on geophysical surveys (Holbrook et al., 2014) and water balance models (Bales et al., 2011; Safeeq and Hunsaker, 2016). Thus, we interpret these low Ge/Si ratios from groundwater and springs to represent near-equilibrium conditions.

We have calculated the equilibrium constant for Ge-kaolinite considering a range of values for both Ge/Si ratios in the fluid and in the clay. The computed values are shown in Figure 1 and Table 1. Here, we have only considered Ge/Si fluid ratios between 0.01 to 0.3 µmol/mol, because Ge/Si ratios from springs and groundwater are well constrained within this range (Lugolobi et al., 2010; Aguirre et al., 2017; Aguirre, 2019). Values > 0.3 in uncontaminated rivers reflect dissolution of secondary clays (Froelich et al., 1992; Kurtz et al., 2002) or additional Ge-enriched sources such as dissolution of phases with high Ge/Si such as sulfides or amphiboles (Anders et al., 2003; Lugolobi et al., 2010). Increasing weathering intensity can result in dissolution of Ge-rich secondary clays (Lugolobi et al., 2010) and drive stream waters to higher Ge/Si (Froelich et al., 1992). Consequently the lowest $(Ge/Si)_{stream}$ values are likely to be the best estimate of the equilibrium fractionation resulting from kaolinite neoformation.

Figure 1 shows that the calculated equilibrium constant for Ge-kaolinite is in the range of 10^2 to $10^{4.5}$ for $(Ge/Si)_{fluid}$ ratios between 0.02 to 0.3 µmol/mol. The different curves show the trajectories for a range of Ge/Si ratios in the clay. It is worth noting that once $(Ge/Si)_{fluid}$ ratios are less than 0.1, they become less sensitive to changes in the equilibrium constant. The results from Figure 1 demonstrate that Ge-kaolinite is necessarily a much less soluble phase compared to Si-kaolinite. Considering that the equilibrium for the hydrolysis of kaolinite (Equation 3) is equal to $10^{6.47}$ (Thermoddem), the calculated solubility for Ge-kaolinite is smaller by 2 to 4 orders of magnitude, consistent with expectations. Based on the solid-solution model for Ge and Si equilibrium fractionation in kaolinite, the recommended values for the Gibbs energy of formation for Ge-kaolinite ΔG_f° and its hydrolysis constant ${}^{Ge}K_{sp}$ are summarized in Table 1.

The predicted Gibbs energy of formation for Ge-kaolinite for that same interval ranges between -3145 to -3120 kJ/mol. The difference between the ΔG_f° for Ge-kaolinite and kaolinite—which equals -3793.9 kJ/mol (Blanc et al., 2012)—, is constrained to ${}^{Ge}\Delta G_f^\circ -$

${}^{Si}\Delta G_f^\circ$ = 650–670 kJ/mol. It is important to note that the sign and difference is comparable to measured and predicted values for other phyllogermanates and their corresponding phyllosilicate phases (Medvedev et al., 1981; Shtenberg et al., 2017). These authors reported the difference for $Ge_2O_5^{2-}$ type germanates with respect to $Si_2O_5^{2-}$ silicates ranges between 603 to 667 kJ/mol. Although the relationship between the available thermodynamic data for this type of phyllogermanates and the aluminogermanate clays—like Ge-kaolinite—might not be identical, the sign and range for the difference between these and their silicate counterparts is systematic: mean $\Delta_{GeG-SiG} \sim 620$ kJ for 2 atoms of Ge in the structure and $\Delta_{GeG-SiG} \sim 340$ kJ for 1 atom of Ge. These data indicate that overall the phyllogermanate phases have a formation Gibbs energy that is 300–350 kJ larger for each mole of Ge in the mineral structure. Assuming that the most representative value for the $(Ge/Si)_{kaolinite}$ is ~ 5.4 (Lugolobi et al., 2010; Aguirre et al., 2017) and for $(Ge/Si)_{fluid} = 0.1$ µmol/mol (Aguirre, 2019), the ${}^{Ge}K_{sp} \approx 10^{3.071}$ and ${}^{Ge}\Delta G_f^\circ \approx -3132$ kJ/mol. Thus, the predicted equilibrium and ΔG_f° results from $(Ge/Si)_{fluid}$ in Figure 1 are consistent with available data for phyllogermanates given the uncertainties.

2.2. Parametric estimation of Ge-kaolinite ΔH°_f, S_f° and ΔG_f°

The parametric method proposed by Blanc et al. (2015) to estimate clay thermodynamic data is based on two independent calculations for ΔH°_f and S°_f. Formation enthalpies of phyllosilicates are calculated as the sum of the enthalpies of constituent oxides—classical approach by Tardy and Garrels (1977)—corrected by a specific term accounting for the interactions of cations with the oxygen atoms in each crystallographic site (Vieillard, 1994). The correction term is based on the empirical parameter $\Delta_H O^= M^{z+}_{i_{(site)}}$, which is derived from known enthalpies of formation of the constituent oxides and crystallographic properties of cations within each mineral group (Vieillard and Tardy, 1988) and has been developed for different types of clays (1:1, 2:1 and 2:1:1). The parameter $\Delta_H O^= M^{z+}_{i_{(site)}}$ has been determined for several cations occupying a specific clay site (i.e. interlayer, tetrahedral, octahedral and brucitic sheets). For elements not considered in the parametrization, this parameter is extrapolated by a linear regression (Blanc et al., 2015). Thus, $\Delta_H O^= M^{z+}_{i_{(site)}}$ can be extrapolated for elements such as Ge in tetrahedral sites. Formation entropies and

heat capacity functions are calculated similarly using a correction parameter. However, the $\Delta_S O^{=} M^{z+}_{i_{(site)}}$ and $\Delta_{C_p} O^{=} M^{z+}_{i_{(site)}}$ parameters are obtained by polyhedral decomposition instead of directly from crystallographic properties, but can be extrapolated to other elements by a linear regression as well. The capacity to include other uncommon elements—usually present as traces—is an advantage of the method proposed by Blanc et al. (2015) compared to other commonly used predictive methods (e.g. Tardy and Garrels, 1977; Helgeson et al., 1978; Chermak and Rimstidt, 1989; Holland, 1989).

Here we have estimated the formation enthalpy and entropy for $Ge_2Al_2O_5(OH)_4$ using the regressions obtained by Blanc et al. (2015) (their equations 30 and 34) to extrapolate the structural $\Delta_H O^{=}$ and $\Delta_S O^{=}$ parameters for Ge^{4+}. Using $GeO_{2(\mathrm{hex})}$ and $Ge^{4+}_{(\mathrm{aq})}$ thermodynamic data (Pokrovski and Schott, 1998; Arnorsson, 1984) we have calculated both enthalpy and entropy correction parameters for Ge in the tetrahedral site ($\Delta_H O^{=} Ge^{4+}_{(IV)}$ and $\Delta_S O^{=} Ge^{4+}_{(IV)}$) to estimate the formation enthalpy and entropy for Ge-kaolinite (Table S1). The Gibbs free energy of formation for Ge-kaolinite was estimated combining the formation enthalpy and entropy calculated previously at standard state (T = 298.15 K, P = 0.1 MPa) and the equilibrium constant for Ge-kaolinite hydrolysis (Equation 2) is calculated using ΔG_f° for Ge-kaolinite and the same data for aqueous species as above (Pokrovski and Schott, 1998; Blanc et al., 2012). Note that the calculation of the Gibbs free energy of formation (ΔG_f°) follows the convention adopted by frequently used databases—such as SUPCRT92, SUPCRTBL and Thermoddem (Johnson et al., 1992; Blanc et al., 2012; Zimmer et al., 2016)—in which it differs in scale from the so called "apparent" Gibbs energy by a constant given by the entropies of the constituent elements (Berman, 1988; Dolejs, 2013). The free aqueous species and constituent oxides data used here is from Thermoddem and it is consistent with the values used by Blanc et al. (2015) for their parametrization. The results for ΔH_f°, S_f° and ΔG_f° are displayed in Table 2.

To assess the uncertainty of our thermodynamic results, we have conducted a Monte Carlo simulation ($n = 10,000$) considering the error in the thermodynamic data for $GeO_{2(\mathrm{hex})}$ and $Ge(OH)_{4(\mathrm{aq})}$ reported by Pokrovski and Schott (1998) and assuming an error in the regression coefficients to calculate the $\Delta^{=}$ parameters. The residuals for these regression coefficients are very small because they have been optimized to minimize the difference between predictions

and calorimetric data (Blanc et al., 2015). This makes it difficult to assess the uncertainty in the regressed $\Delta_H O^=$ and $\Delta_S O^=$ parameters for enthalpy and entropy. According to Blanc et al. (2015) the parametric method overestimates ΔH_f° while it underestimates S_f° and thus these uncertainties tend to decrease the overall uncertainty of the computed ΔG_f°. Therefore, to evaluate the error produced by the uncertainty in the regression coefficients for both $\Delta_H O^=$ and $\Delta_S O^=$ we have assumed a 0.7% error in the linear model coefficients. This approach aims to assess the overall uncertainty on the regressed parameters for Ge, since the parametrization of Blanc et al. (2015) did not include Ge-bearing aluminosilicates for obvious reasons—lack of data—which can have an important effect in the determined ΔG_f° values and K_{sp}.

The estimated thermodynamic properties for Ge-kaolinite yield a higher $\Delta G_f^\circ = -3094.03$ value by 1% than the predicted range from natural samples (Figure 1). For this estimated thermodynamic data, the modeled equilibrium for Ge-kaolinite hydrolysis (Equation 2) is equal to $10^{9.30}$, i.e. predicting a less soluble phase than Si-kaolinite, consequently reversing the observed sense of fractionation. It is important to emphasize that although the ${}^{Ge}K_{sp}$ remains experimentally undetermined, this value cannot be larger than ${}^{Si}K_{sp}$, as it would reverse the partitioning sense, contradicting the large body of evidence that Ge is preferentially fractionated into secondary minerals during weathering. This result reflects an overestimation of ΔG_f°, and therefore ${}^{Ge}K_{sp}$, that is within the uncertainty of the original thermodynamic data, and the $\Delta_H O^=$ and $\Delta_S O^=$ parameters for Ge in the parametric method—that we have assumed to be 0.7%. Note that it is hard to assess whether this is an overestimation of ΔH_f° or underestimation of S_f°. Alternatively, it is possible that there is no equilibrium partitioning between both elements in kaolinite and that observed ratios are just a result of favorable kinetics for incorporation of Ge into secondary clays—thus, implying that a solid-solution between Ge and Si does not exist. This might be possible, since the dissociation energy of $Ge(OH)_{4(aq)}$ is lower than for silicic acid (Pokrovski and Schott, 1998). However, the observation that the lowest observed Ge/Si fluids are found in groundwaters with long residence times argues against such an interpretation.

The difference between the predicted ΔG_f° for Ge-kaolinite with its Si counterpart is 700 kJ/mol, compared with the 664 $\pm$10 kJ/mol derived from the empirical approach. This

difference is also larger by $>$ 30 kJ than differences observed in the only published values for phyllogermanates with respect to their Si-counterparts (603–667 kJ/mol). The apparent 30–40 kJ overestimation in the ΔG_f° of Ge-kaolinite from the parametric method is important, as the equilibrium constant for Ge-kaolinite hydrolysis can change up to 2 orders of magnitude by every 10 kJ difference in the Gibbs energy of the reaction. Blanc et al. (2015) point out that the extrapolation with their model becomes less accurate for extreme compositions and elements outside the parametrization, such as the case of Ge-kaolinite ($Ge_2Al_2O_5(OH)_4$) calculated here. This implies that a $\pm$ 0.7% uncertainty in both $\Delta_H O^=$ and $\Delta_S O^=$ can account for the error in ΔG_f°. We argue that 30–40 kJ overestimation of the ΔG_f° for Ge-kaolinite from the parametric method (-3094.03 kJ/mol) compared to values obtained for groundwater samples (-3140 to -3125 kJ/mol) is within the uncertainty of the thermodynamic data and the extrapolation of the $\Delta_H O^=$ and $\Delta_S O^=$ parameters. Finally, it should be stated that the configurational entropy (S_{conf}) of Ge-kaolinite has been assumed equal to zero—i.e. there is no disorder in the tetrahedral site. However, if $S_{conf} > 0$, then the ΔG_f° of Ge-kaolinite should be < -3094.03, which would be consistent with the results obtained in section 2.1. We note that this case would imply some degree of non-ideal mixing; however, this has not been observed in phyllosilicates (Martin et al., 1992, 1996). Additional thermodynamic data could resolve the discrepancy between the results of the parametric model and the empirical results, as well as enable a wide range of compositions to be treated effectively.

3. Numerical experiments on Ge/Si fractionation during precipitation of kaolinite

3.1. Batch dissolution and precipitation model for Ge/Si fractionation

We can use the modeled equilibrium partitioning data calculated in Section 2 to understand the dynamics of Ge/Si fractionation in natural systems. We first evaluate the role of re-equilibration of Ge/Si ratios between the the fluid and the precipitated solids. Our second goal is to test how the kinetics of feldspar dissolution—supplying Ge and Si to solution—and kaolinite precipitation could impact Ge/Si ratios in real systems. There are a number of different rate laws for kaolinite dissolution and precipitation with different reaction orders and

linear or non-linear dependence on affinity ($\log(Q/K_{eq})$) (Carrollwebb and Walther, 1988; Carroll and Walther, 1990; Nagy et al., 1991; Chin and Mills, 1991; Ganor et al., 1995; Devidal et al., 1997; Huertas et al., 1998, 1999; Metz and Ganor, 2001; Cama et al., 2002; Yang and Steefel, 2008). Some of them suggest that kaolinite dissolution/precipitation can be modeled by a reversible reaction as a function of the rate constant, surface area and the affinity term. This type of rate law formulation has been derived by Lasaga (1981) and it is often referred as "TST" formulation because is a derivation from Transition State Theory (e.g. Aagaard and Helgeson, 1982; Steefel et al., 2015). Other suggest that kaolinite precipitation should be described by non-reversible (or "non-TST") formulations (e.g. Yang and Steefel, 2008). The heterogeneity of rate laws probably arises from the difficulty of carrying out suitable low-temperature clay precipitation experiments particularly when the system is close to saturation (e.g. Zhu et al., 2020). In this section we seek to determine which type of formulation can predict results that are in plausible agreement with observations from natural systems.

We have set up a batch dissolution and precipitation model using the geochemical reactive transport code CrunchFlow (Steefel et al., 2015). The model is initialized with a single-mineral porous media consisting of a solid solution between albite ($NaAlSi_3O_8$) and Ge-albite ($NaAlGe_3O_8$), represented by $NaAl(Si_{(1-x)}Ge_x)_3O_8$ with a Ge/Si ratio of 1.5 µmol/mol (Lugolobi et al., 2010), thus with a Ge activity $a_{Ge} = 4.5 \times 10^{-6}$. Note here, that by using a single mineral solid-solution for the dissolving phase, we have assumed that Ge-Si fractionation during dissolution of feldspars does not occur, which is consistent with the general observation that Ge/Si in streams are controlled by precipitation and dissolution of secondary minerals (Murnane and Stallard, 1990; Froelich et al., 1992; Kurtz et al., 2002). Additionally, the amount of Ge released by rock weathering should only depend on the concentration of Ge in the rock, which is determined by its mineral assemblage (Evans and Derry, 2002).

The initial mineral volume fraction is 35%, implying a W/R = 2. The fluid velocity and diffusion coefficient are set equal to zero in the batch reactor. The initial composition of the fluid has a Ge/Si = 1 (µmol/mol) and the initial pH set to 6 (Table S2). In our model, dissolution and precipitation of minerals are described by reversible reactions with a linear

or non-linear dependence on the saturation state (TST-type). Thus, the dissolution and precipitation of the minerals in the system follows:

$$R_{(mol/m^3/s)} = -A_{bulk} \times k\left[1 - \left(\frac{Q}{K_{sp}}\right)^{n_1}\right]^{n_2} \tag{7}$$

where A is the surface area, k is the rate constant and Q/K_{sp} is the saturation index. In this simulation albite dissolution only follows a linear dependence (n_1 and $n_2 = 1$, where n_1 is the inverse of the Temkin coefficient) on the affinity term, as the fluid is undersaturated with respect to albite ($\log(Q/K_{eq}) \approx -10$) (Table 5 in Marty et al., 2015). Zhu et al. (2020) suggested that albite dissolution can also be represented with an irreversible linear rate law; and the approach here—given the degree of undersaturation (Figure 3)—provides the same results. For the purpose of studying a formulation that agrees with Ge/Si observations from natural systems, we had to make several assumptions about the precipitation kinetics of kaolinite. For both the Si and Ge end-members of kaolinite we used both linear-TST (e.g. Carrollwebb and Walther, 1988; Carroll and Walther, 1990; Ganor et al., 1995; Cama et al., 2002; Marty et al., 2015) and non-linear-TST with $n_1 = 0.5$ formulations for dissolution with a weaker dependence on the affinity term (Nagy et al., 1991; Devidal et al., 1997; Yang and Steefel, 2008) and assumed these are valid for precipitation (Table 5 in Marty et al., 2015). Additionally, we also compare these results with rate laws derived explicitly for kaolinite precipitation: the first is a the parametrization derived from experimental data (Nagy et al., 1991; Yang and Steefel, 2008) by Marty et al. (2015) (their Table 8) and the second is the experimental formulation by Yang and Steefel (2008), which describes no back-reaction close to equilibrium. The rate constants (k_f) used here were obtained directly from Marty et al. (2015) or as distributed with the CrunchFlow package for those from Yang and Steefel (2008). These values are summarized in Table 3, including details on rate-law parameters and surface areas used for this modeling experiment. A_{bulk} is updated for each mineral in terms of their volume fraction, molar volume and molar weight.

The solid-solution model for $(Si_{1-x}Ge_x)_2Al_2O_5(OH)_4$ is represented in CrunchFlow as two different minerals with end-member compositions with separate rate laws (Druhan et al., 2013; Steefel et al., 2014):

$$ {}^{Ge}R_{net} = X_{Ge}^2 \, {}^{Ge}k_f \, {}^{Ge}K_{sp} \left[\left(\frac{a^2_{\mathrm{Ge(OH)_4}} a^2_{\mathrm{Al^{3+}}}}{a^6_{\mathrm{H^+}} X^2_{Ge}} \frac{1}{{}^{Ge}K_{sp}} \right)^{n_1} - 1 \right] \tag{8} $$

$$ {}^{Si}R_{net} = X_{Si}^2 \, {}^{Si}k_f \, {}^{Si}K_{sp} \left[\left(\frac{a^2_{\mathrm{Si(OH)_4}} a^2_{\mathrm{Al^{3+}}}}{a^6_{\mathrm{H^+}} X^2_{Si}} \frac{1}{{}^{Si}K_{sp}} \right)^{n_1} - 1 \right] \tag{9} $$

where ${}^{Ge}k_f$ and ${}^{Si}k_f$ are the precipitation (forward) rate constants, ${}^{Ge}K_{sp}$ and ${}^{Si}K_{sp}$ the solubility constants, $X_{Ge} = x$ and $X_{Si} = 1 - x$ are the mole fractions of Ge-kaolinite and kaolinite respectively, a_n is the activity of the species n, and n_1 is the dependence on affinity. Note that to use CrunchFlow's solid-solution model (Equations 8 and 9) all rate laws have to be assumed of the TST-type. The rates describing each mineral are coupled by the activity of each mineral—i.e. through the mole fraction term. Equilibrium fractionation is directly implied by the different equilibrium constants (Equation 6) and kinetic fractionation can be represented by a kinetic fractionation factor equal to the ratio between the rate constants for the Ge and Si kaolinite end-members: $\alpha_k = {}^{Ge}k_f / {}^{Si}k_f$. Equations 8 and 9 imply that re-equilibration of the bulk solid and the fluid occurs; i.e. the composition of the solid phase will affect the affinity term (Q/K_{sp}) and both Ge and Si can continue to exchange between the fluid and the solid despite reaching mineral saturation for kaolinite—$R_{net} = 0$ (Druhan et al., 2013). However, re-equilibration of Ge/Si ratios between fluid and kaolinite in natural systems has not been shown to occur to the same extent and at sufficiently fast rates as observed for divalent cations in carbonates (Gabitov and Watson, 2006; Gabitov et al., 2014) and sulfates (Putnis et al., 1992; Prieto et al., 1997). This is given the progressively more depleted values found in groundwater (Aguirre, 2019) and the elevated Ge/Si ratios found in kaolinite (Kurtz et al., 2002; Lugolobi et al., 2010; Aguirre et al., 2017). Moreover, Evans and Derry (2002) modeled Ge-Si partitioning in quartz precipitation as Rayleigh fractionation, suggesting that re-equilibration between both phases does not take place. If re-equilibration does not occur, the saturation states corrected by the ratio of the equilibrium constants are equal for the Ge and Si end-members (Steefel et al., 2014). This is equivalent to:

$$ \frac{1}{{}^{Ge}K_{sp}} \frac{a^2_{\mathrm{Ge(OH)_4}} a^2_{\mathrm{Al^{3+}}}}{a^6_{\mathrm{H^+}} X^2_{Ge}} = \frac{1}{{}^{Si}K_{sp}} \frac{a^2_{\mathrm{Si(OH)_4}} a^2_{\mathrm{Al^{3+}}}}{a^6_{\mathrm{H^+}} X^2_{Si}} \tag{10} $$

in which case the activity of Ge and Si in the solid-solution does not affect the net rate and

the rate controlling equation can be re-written just in terms of the fluid Ge/Si ratio:

$$^{Ge}R_{net} = (Ge/Si)^2_{fluid}\,{}^{Ge}k_f\,{}^{Ge}K_{sp}\left(\frac{Q_{kaolinite}}{{}^{Ge}K_{sp}} - 1\right) \tag{11}$$

using the substitution $\frac{a_{\mathrm{Ge(OH)_4}}}{a_{\mathrm{Si(OH)_4}}} = (Ge/Si)_{fluid}$. Here, $Q_{kaolinite}$ is the ion solubility product for $Al_2Si_2O_5(OH)_4$, $X_{Si} \approx 1$ and for simplicity we used $n_1 = 1$.

This formulation is similar to the one obtained by DePaolo (2011) by assuming an steady-state mineral surface composition for Sr/Ca partitioning in calcite. It is implied that equation (11) is only valid until the fluid becomes saturated with respect to kaolinite—i.e. $Q_{kaolinite} = {}^{Si}K_{sp}$. Equilibrium constants (K_{sp}) used for albite and kaolinite are from the Thermoddem database (Table 3). For Ge-kaolinite, the equilibrium constant was determined in section 2.1 for $\Delta {G_f}^{\circ}{}_{(Ge-kaolinite)} = -3130$ kJ/mol, which corresponds to an equilibrium fractionation coefficient $D'_{Ge-Si} = 4 \times 10^{-4}$ (Figure 2).

3.2. Equilibrium partitioning for a linear TST reaction rate law

The batch simulations are constructed from a base model for which $D'_{Ge-Si} = 4 \times 10^{-4}$, a linear TST precipitation rate with no kinetic fractionation, no re-equilibration (Equation 11) and with initial fluid composition in Table S2. The simulation is run for 1–50 years to keep track of the evolution of Ge/Si ratios in the fluid and in the newly precipitated mineral solid-solution. The batch reactor with initial $(Ge/Si)_{fluid} = 1$ (µmol/mol) reacting with a Ge-albite solid solution shows that Ge is preferentially incorporated into kaolinite, while the fluid becomes depleted in Ge (Figure 4). The Ge/Si ratios in the fluid initially increase up to 1.2 µmol/mol and decrease as precipitation of the solid starts at $\sim$ 10 days. The strong Ge/Si partitioning results in an initial solid with high Ge/Si ($\approx$ 60 µmol/mol) in this period. As the reaction progresses Ge/Si ratios in the fluid rapidly decrease to $\sim$ 0.04 (µmol/mol); while the Ge/Si ratio in kaolinite settles to $\sim$ 5.2 µmol/mol after 1 year. Steady-state is obtained after sufficiently long time—more than 10 years— when the solid reaches at $\sim$ 4.5 µmol/mol (Figure S1) and the fluid is at $\sim$ 0.05 µmol/mol.

The predicted equilibrium $(Ge/Si)_{fluid}$ ratios are lower than most values measured from rivers (i.e. Mortlock and Froelich (1987)). However, these are equivalent to values obtained from groundwater in a granitic catchment showing sufficiently long transit times (Aguirre,

2019). The modeled equilibrium $(Ge/Si)_{kaolinite}$ values are comparable to those measured by many studies (Kurtz et al., 2002; Lugolobi et al., 2010; Qi et al., 2019). Higher Ge/Si ratios in the solids will result from higher initial concentrations of Ge in the parent materials—e.g. basalts and other igneous rocks with higher contents of hornblende and biotite—and reacting fluids with higher Ge concentrations. We have shown how kaolinite can produce fractionation of Ge from fluids, however the timescales at which this process occurs can depend on several intrinsic or extrinsic factors in natural systems.

3.3. Discrepancy between riverine and predicted Ge/Si fluid ratios

Ge/Si ratios from unpolluted rivers are usually higher ($\sim$ 0.35 µmol/mol, Mortlock and Froelich, 1987; Baronas et al., 2018) than the predicted values from our equilibrium fractionation batch reactor model. There are several explanations for this discrepancy including extrinsic and intrinsic factors to the secondary-clay precipitation system. First, elemental concentrations in rivers often represent the mixing of several sources and water parcels with different transit times and multiple pathways. Dissolution of primary minerals phases with variable Ge/Si, colloidal transport, dissolution of secondary clays and oxides, and biogenic cycling of Ge and Si can all impact Ge/Si ratios in soil and waters in the vadose zone (e.g. Anders et al., 2003; Derry et al., 2005; Cornelis et al., 2010; Lugolobi et al., 2010; Aguirre et al., 2017; Ameijeiras-Marino et al., 2018). This implies that the fraction of water carrying low Ge/Si ratios representing secondary clay formation that is supplied to streams will vary depending on hydrologic conditions, resulting in time- and discharge-related variation in stream Ge/Si ratios (Kurtz et al., 2011).

On the other hand, intrinsic factors controlling kaolinite—or secondary clays—precipitation can also explain to some degree the variability observed in natural systems. For example the base model does not account the effect of re-equilibration of the precipitated solid with the fluid. Moreover, the nature of dissolution and precipitation kinetics, including controlling rate laws and effective surface areas, can play a strong influence in the transient or "short-term" behavior of Ge/Si ratios in fluids and solids. The precipitation dynamics of kaolinite will likely influence the function of Ge/Si ratios in the environment. Both intrinsic (precipitation dynamics, kinetics and partitioning coefficients) and extrinsic (pH, W/R ratios)

factors have direct control on the net precipitation rate of kaolinite. In the next section we will discuss the effects of the re-equilibration and kinetic controls and their relevance to observations from weathering systems including soils and streams.

3.3.1. The effect of re-equilibration on Ge/Si ratios

The models above do not consider re-equilibration of Ge/Si ratios between the fluid and the precipitated solid. Trace element exchange at low temperatures has been shown to occur in carbonates between Ca and other divalent cations such as Sr (Gabitov and Watson, 2006; Gabitov et al., 2014) or Cd (e.g Prieto et al., 1997). This phenomena has also been observed for Ra during re-crystallization of barite (Curti et al., 2010). Thus, it is plausible to consider that Ge and Si continue to exchange between the fluid and the mineral at longer timescales in pseudo-closed systems. When re-equilibration is allowed in this batch model, the mineral mole fractions of Ge and Si influence the affinity term and the precipitation of the solid follows equation 8. The continuous exchange of Ge and Si between the mineral solid-solution and the fluid results in higher $(Ge/Si)_{fluid}$ ratios that reach 0.44 µmol/mol, with a more depleted solid at $(Ge/Si)_{solid} \sim 4.2$ µmol/mol (Figure 5) after 1 year of reaction. At steady-state (Figure S2), the Ge/Si ratios in the fluid and solid are considerably different between the models with and without re-equilibration: after 50 years of reaction the fluid reaches a $(Ge/Si)_{fluid} = 0.5$ µmol/mol with $(Ge/Si)_{solid} = 3.5$ µmol/mol. Note here that re-equilibration is calculated with respect to the bulk solid, which probably overstimates the extent to which this mechanism occurs (Druhan et al., 2013; Steefel et al., 2014). Mineral zonation between Ge and Si from re-equilibration in silicate minerals likely occurs, much like in the Ca-carbonate and Ba-sulfate systems (Prieto, 2009; Prieto et al., 2016). For example, Fernandez et al. (2019) showed that Si-isotopes undergo re-equilibration in neoformed opal crystals, but the depth-extent of this interaction is limited by reaction rates, leading to a zoned crystal. Thus, we hypothesize that re-equilibration of Ge/Si ratios in kaolinite must occur, but this effect is rather limited given the slow kinetics of kaolinite precipitation in surface environments in comparison to carbonate or sulfate systems. Given the substantially lower values found in groundwater and springs (Aguirre, 2019) and the overall evidence of lower $(Ge/Si)_{fluid} < 0.35$ µmol/mol from in unpolluted rivers (Mortlock and Froelich, 1987;

Baronas et al., 2018) it seems that re-equilibration is a limited process during Ge/Si partitioning, potentially analogous to that observed for Si isotopes in amorphous silica precipitation experiments (Fernandez et al., 2019).

3.3.2. Kaolinite precipitation rate controls the short-term Ge/Si response in fluids

Since partitioning of Ge from a fluid is controlled by its incorporation into secondary clays, the precipitation rate of minerals like kaolinite will influence the speed at which Ge is removed from the fluid. Therefore, when the kinetics of precipitation are not efficient, Ge can build up in the fluid before it starts to precipitate in (pseudo)-closed systems. There has been a long debate about discrepancies between laboratory versus field measured weathering rates and often field rates are 2 to 5 orders of magnitude slower than laboratory experiments (White and Brantley, 2003; Maher et al., 2006). For the idealized system modeled here, kaolinite supersaturation (Figure 3) can have a strong effect on the precipitation rate. However, close-to-equilibrium systems can be best described by a rate law with a non-linear dependence on the reaction affinity term (Maher et al., 2009), and/or by a non-TST rate law (Yang and Steefel, 2008). We evaluated the effects of different rate formulations (Table 3) including non-linear TST and non-TST formulations (Figures 6 and S3). The non-linear TST formulation assumes the rate constant and n_1 and n_2 coefficients (Eq. 7) for kaolinite dissolution based on Yang and Steefel (2008). We also used formulations derived exclusively for precipitation: (1) The non-linear regressed parameters by Marty et al. (2015)—which are in turn, based on the experiments by Nagy et al. (1991), Devidal et al. (1997) and Yang and Steefel (2008); and (2) the formulation derived directly from the experiment by Yang and Steefel (2008). As we said before, a limitation of CrunchFlow's isotope block is that it can only be used with reversible (TST) rate laws. This means that for the non-TST numerical experiment, we have assumed it behaves as TST, but we called it non-TST model to identify this formulation consistently.

The non-linear and non-TST precipitation rate laws imply that the precipitation kinetics are less dependant on the reaction affinity, and thus the $(Ge/Si)_{fluid}$ ratios can build up before precipitation begins. Using the non-linear—and non-TST—rate laws for the precipitation of kaolinite, Ge/Si ratios in the fluid can reach above 0.8 µmol/mol after one year

(Figures 6). The Ge/Si ratios in the solid show almost no fractionation—$(Ge/Si)_{solid} \approx 1$ µmol/mol—for the two precipitation formulations; whereas the non-linear TST by Yang and Steefel (2008) shows high $(Ge/Si)_{solid}$ above 10 µmol/mol. This appears to be a delayed response compared to the linear-TST rate law, i.e. high initial $(Ge/Si)_{solid}$ ratios. At longer timescales ($>$ 50 years), the non-linear TST rate formulation of Yang and Steefel (2008) shows the expected partitioning behavior of Ge/Si ratios between the fluid and kaolinite (Figure S3), with Ge/Si ratios within those predicted by the linear-TST. However, both precipitation non-linear and non-TST formulations are too slow to show significant partitioning, and thus, cannot reproduce the observations from weathering systems (e.g. Froelich et al., 1992; Kurtz et al., 2002; Lugolobi et al., 2010; Baronas et al., 2018).

Although the timescales of our batch-reaction models are hypothetical, the fact is that Ge/Si fractionation during secondary clay precipitation is observed in natural systems governed by the timescale of water residence times (Aguirre, 2019). Thus, we hypothesize that slow precipitation dynamics cannot capture the behavior of Ge/Si partitioning, as it would require disproportionately long water residence times, even in systems dominated by large fractions of these older water parcels (Rademacher et al., 2005). Recent advances on the hydrology of natural systems indicate that in most catchments and the whole critical zone the fraction of water parcels older than 1 year is small, according to models of water transit times distribution and age tracer data (e.g. Jasechko et al., 2016; Benettin et al., 2017; Sprenger et al., 2019). The apparent contradiction between observed Ge/Si ratios in natural systems and the "slow-precipitation" models highlights the need of using isotopic or trace element tracers in clay precipitation experiments to better constrain precipitation mechanisms, an approach that has shown promising results in close-to-equilibrium dissolution experiments (Zhu et al., 2020).

4. Concluding remarks

Our model results provide a consistent framework that describes Ge-Si partitioning during chemical weathering, represented here by plagioclase dissolution and kaolinite precipitation. We have determined the Gibbs free energy and solubility constant for a theoretical Ge-bearing kaolinite (Ge-kaolinite) using an ideal solid-solution model and a direct calcula-

tion from field-measured Ge/Si ratios found in kaolinite and Ge-depleted groundwaters in equilibrium with kaolinite. We also estimated Ge-kaolinite thermodynamic properties using a parameterization approach that rendered higher ΔG_f° and K_{sp} values which reversed the fractionation sense, contradicting the evidence available from field observations. This contradiction reflects the inherent uncertainty in this method, but additional thermodynamic data could resolve this issue. Although the actual value of the germanium partitioning coefficient for kaolinite and weathering fluids remains uncertain, we have provided an estimated range for the distribution coefficient of $10^{-4} < D'_{Ge-Si} < 10^{-2}$ based on Ge/Si ratios observed in kaolinites from several locations and in groundwaters that have long residence times. This refines the partition coefficient determined by Froelich et al. (1992) based on overall higher Ge/Si ratios in rivers. Our results provide a consistent framework that should be widely applicable. Geochemical models and reactive transport codes can use the Ge-kaolinite solubility constant derived here directly, or use it to calculate the K_{sp} for specific Ge/Si compositions based on the solid-solution model. Since Ge/Si ratios have proven to be an unique tracer of the terrestrial Si-cycle, our study stresses the need for future experimental studies to synthesize Ge-bearing clays, such as $Ge_2Al_2O_5(OH)_4$, and to further determine their thermodynamic properties to get better constraints on this system.

Our Ge-Si solid solution model can be used to study the effect of weathering in the global Si cycle. The batch dissolution and precipitation numerical experiments show how mineral precipitation dynamics can influence the partitioning of Ge and Si in fluids and secondary minerals. These models show that both precipitation rate laws for kaolinite, as well as re-equilibration control the far-from-equilibrium behavior of Ge/Si ratios at short to middle timescales. Given the uncertainties in kaolinite precipitation dynamics in natural systems, it remains to be explored what these timescales might be. We suggest that further studies should combine groundwater dating methods with Ge/Si ratios to elucidate these answers.

Acknowledgements

This project was conducted at IPGP as part of research stay made by A.P. A.P thanks Jerome Gaillardet and the G2E team for hosting her during this research stay. We would like to thank Jennifer Druhan for assistance with CrunchFlow's isotope block. This research

is funded by Campus France's "Make Our Planet Great Again" short-stay program and the IAGC Student Grant awarded to A.P. L.A.D acknowledges ANR Program "Investissements d'avenir" ANR-17-MPGA-0009 and U.S. NSF EAR-1349269 grants. A.P acknowledges CONICYT PFCHA/Doctorado Becas Chile/2014 - 72150180 for PhD fellowships. We used Peter Kovesi's Colorcet Matlab package for perceptually uniform color grading plots. We would like to thank the Associate Editor, Sophie Opfergelt, for the diligent handling of the manuscript and suggestions. This manuscript benefited from the detailed and thoughtful reviews by Merlin Méheut and three other anonymous reviewers.

References

Aagaard, P., Helgeson, H.C., 1982. Thermodynamic and kinetic constraints on reaction-rates among minerals and aqueous-solutions .1. Theoretical considerations. American Journal of Science 282, 237–285. doi:10.2475/ajs.282.3.237.

Aguirre, A.A., 2019. Applying Ge/Si Ratios to Trace Weathering Reactions, Hydrologic Pathways and Coal Fly Ash Contamination in Watersheds across the United States. Ph.D. thesis. Cornell University.

Aguirre, A.A., Derry, L.A., Mills, T.J., Anderson, S.P., 2017. Colloidal transport in the Gordon Gulch catchment of the Boulder Creek CZO and its effect on C-Q relationships for silicon. Water Resources Research 53, 2368–2383. doi:10.1002/2016wr019730.

Ameijeiras-Marino, Y., Opfergelt, S., Derry, L.A., Robinet, J., Govers, G., Minella, J.P.G., Delmelle, P., 2018. Ge/Si ratios point to increased contribution from deeper mineral weathering to streams after forest conversion to cropland. Applied Geochemistry 96, 24–34. doi:10.1016/j.apgeochem.2018.06.002.

Anders, A.M., Sletten, R.S., Derry, L.A., Hallet, B., 2003. Germanium/silicon ratios in the Copper River Basin, Alaska: Weathering and partitioning in periglacial versus glacial environments. Journal of Geophysical Research-Earth Surface 108, 10. doi:10.1029/2003jf000026.

Arnorsson, S., 1984. Germanium in Icelandic geothermal waters. Geochimica et Cosmochimica Acta 48, 2489–2502. doi:10.1016/0016-7037(84)90300-4.

Bales, R.C., Hopmans, J.W., O'Geen, A.T., Meadows, M., Hartsough, P.C., Kirchner, P., Hunsaker, C.T., Beaudette, D., 2011. Soil Moisture Response to Snowmelt and Rainfall in a Sierra Nevada Mixed-Conifer Forest. Vadose Zone Journal 10, 786–799. doi:10.2136/vzj2011.0001.

Baronas, J.J., Torres, M.A., West, A.J., Rouxel, O., Georg, B., Bouchez, J., Gaillardet, J., Hammond, D.E., 2018. Ge and Si isotope signatures in rivers: A quantitative multi-proxy approach. Earth and Planetary Science Letters 503, 194–215. doi:10.1016/j.epsl.2018.09.022.

Benettin, P., Bailey, S.W., Rinaldo, A., Likens, G.E., McGuire, K.J., Botter, G., 2017. Young runoff fractions control streamwater age and solute concentration dynamics. Hydrological Processes 31, 2982–2986. doi:10.1002/hyp.11243.

Berman, R.G., 1988. Internally-consistent thermodynamic data for minerals in the system Na2O-K2O-CaO-MgO-FeO-Fe2O3-Al2O3-SiO2-TiO2-H2O-CO2. Journal of Petrology 29, 445–522. doi:10.1093/petrology/29.2.445.

Bernstein, L.R., 1985. Germanium geochemistry and mineralogy. Geochimica et Cosmochimica Acta 49, 2409–2422. doi:10.1016/0016-7037(85)90241-8.

Blanc, P., Lassin, A., Piantone, P., Azaroual, M., Jacquemet, N., Fabbri, A., Gaucher, E.C., 2012. Thermoddem: A geochemical database focused on low temperature water/rock interactions and waste materials. Applied Geochemistry 27, 2107–2116. doi:10.1016/j.apgeochem.2012.06.002.

Blanc, P., Vieillard, P., Gailhanou, H., Gaboreau, S., Gaucher, E., Fialips, C.I., Made, B., Giffaut, E., 2015. A generalized model for predicting the thermodynamic properties of clay minerals. American Journal of Science 315, 734–780. doi:10.2475/08.2015.02.

583 Cama, J., Metz, V., Ganor, J., 2002. The effect of pH and temperature on kaolinite dis-
584 solution rate under acidic conditions. Geochimica et Cosmochimica Acta 66, 3913–3926.
585 doi:10.1016/s0016-7037(02)00966-3.

586 Capobianco, C., Navrotsky, A., 1982. Calorimetric evidence for ideal mixing of silicon and
587 germanium in glasses and crystals of sodium-feldspar composition. American Mineralogist
588 67, 718–724.

589 Carroll, S.A., Walther, J.V., 1990. Kaolinite dissolution at 25-degrees-C, 60-degrees-C, and
590 80-degrees-C. American Journal of Science 290, 797–810. doi:10.2475/ajs.290.7.797.

591 Carrollwebb, S.A., Walther, J.V., 1988. A surface complex-reaction model for the pH-
592 dependence of corundum and kaolinite dissolution rates. Geochimica et Cosmochimica
593 Acta 52, 2609–2623. doi:10.1016/0016-7037(88)90030-0.

594 Chermak, J.A., Rimstidt, J.D., 1989. Estimating the thermodynamic properties (Delta-Gfo
595 and Delta-Hfo) of silicate minerals at 298 K from the sum of polyhedral contributions.
596 American Mineralogist 74, 1023–1031.

597 Chillrud, S.N., Pedrozo, F.L., Temporetti, P.F., Planas, H.F., Froelich, P.N., 1994.
598 Chemical-weathering of phosphate and germanium in glacial meltwater streams - Ef-
599 fects of subglacial pyrite oxidation. Limnology and Oceanography 39, 1130–1140.
600 doi:10.4319/lo.1994.39.5.1130.

601 Chin, P.K.F., Mills, G.L., 1991. Kinetics and mechanisms of kaolinite dissolution - effects of
602 organic-ligands. Chemical Geology 90, 307–317. doi:10.1016/0009-2541(91)90106-2.

603 Cornelis, J.T., Delvaux, B., Cardinal, D., Andre, L., Ranger, J., Opfergelt, S., 2010. Trac-
604 ing mechanisms controlling the release of dissolved silicon in forest soil solutions us-
605 ing Si isotopes and Ge/Si ratios. Geochimica et Cosmochimica Acta 74, 3913–3924.
606 doi:10.1016/j.gca.2010.04.056.

607 Curti, E., Fujiwara, K., Iijima, K., Tits, J., Cuesta, C., Kitamura, A., Glaus, M.A., Muller,
608 W., 2010. Radium uptake during barite recrystallization at 23 +/- 2 degrees C as a function

of solution composition: An experimental Ba-133 and Ra-226 tracer study. Geochimica et Cosmochimica Acta 74, 3553–3570. doi:10.1016/j.gca.2010.03.018.

Delany, J.M., Wolery, T.J., 1989. The LLNL thermochemical database. Report UCRL-21658. Technical Report. Lawrence Livermore National Laboratory.

DePaolo, D.J., 2011. Surface kinetic model for isotopic and trace element fractionation during precipitation of calcite from aqueous solutions. Geochimica et Cosmochimica Acta 75, 1039–1056. doi:10.1016/j.gca.2010.11.020.

Derry, L.A., Kurtz, A.C., Ziegler, K., Chadwick, O.A., 2005. Biological control of terrestrial silica cycling and export fluxes to watersheds. Nature 433, 728–731. doi:10.1038/nature03299.

Devidal, J.L., Schott, J., Dandurand, J.L., 1997. An experimental study of kaolinite dissolution and precipitation kinetics as a function of chemical affinity and solution composition at 150 degrees C, 40 bars, and pH 2, 6.8, and 7.8. Geochimica et Cosmochimica Acta 61, 5165–5186. doi:10.1016/s0016-7037(97)00352-9.

Dolejs, D., 2013. Thermodynamics of aqueous species at high temperatures and pressures: Equations of state and transport theory. Thermodynamics of Geothermal Fluids 76, 35–79. doi:10.2138/rmg.2013.76.3.

Druhan, J.L., Steefel, C.I., Williams, K.H., DePaolo, D.J., 2013. Calcium isotope fractionation in groundwater: Molecular scale processes influencing field scale behavior. Geochimica et Cosmochimica Acta 119, 93–116. doi:10.1016/j.gca.2013.05.022.

Evans, M.J., Derry, L.A., 2002. Quartz control of high germanium/silicon ratios in geothermal waters. Geology 30, 1019–1022. doi:10.1130/0091-7613(2002)030<1019:qcohgs>2.0.co;2.

Fernandez, N.M., Zhang, X., Druhan, J.L., 2019. Silicon isotopic re-equilibration during amorphous silica precipitation and implications for isotopic signatures in geochemical proxies. Geochimica et Cosmochimica Acta 262, 104–127. doi:10.1016/j.gca.2019.07.029.

635 Froelich, P.N., Blanc, V., Mortlock, R.A., Chillrud, S.N., Dunstan, W., Udomkit, A., Peng,
636 T.H., 1992. River fluxes of dissolved silica to the ocean were higher during glacials: Ge/Si
637 in diatoms, rivers, and oceans. Paleoceanography 7, 739–767. doi:10.1029/92pa02090.

638 Froelich, P.N., Hambrick, G.A., Andreae, M.O., Mortlock, R.A., Edmond, J.M., 1985. The
639 geochemistry of inorganic germanium in natural waters. Journal of Geophysical Research-
640 Oceans 90, 1133–1141. doi:10.1029/JC090iC01p01133.

641 Gabitov, R.I., Sadekov, A., Leinweber, A., 2014. Crystal growth rate effect on Mg/Ca and
642 Sr/Ca partitioning between calcite and fluid: An in situ approach. Chemical Geology 367,
643 70–82. doi:10.1016/j.chemgeo.2013.12.019.

644 Gabitov, R.I., Watson, E.B., 2006. Partitioning of strontium between calcite and fluid.
645 Geochemistry Geophysics Geosystems 7, 12. doi:10.1029/2005gc001216.

646 Ganor, J., Mogollon, J.L., Lasaga, A.C., 1995. The effect of pH on kaolinite dissolu-
647 tion rates and on activation-energy. Geochimica et Cosmochimica Acta 59, 1037–1052.
648 doi:10.1016/0016-7037(95)00021-q.

649 Goldschmidt, V.M., 1926. Concerning the crystallo-chemical and geochemical behaviour of
650 Germanium. Naturwissenschaften 14, 295–297. doi:10.1007/bf01503585.

651 Helgeson, H.C., Delany, J.M., Nesbitt, H.W., Bird, D.K., 1978. Summary and critique of
652 the thermodynamic properties of rock-forming minerals. American Journal of Science 278,
653 1–229.

654 Holbrook, W.S., Riebe, C.S., Elwaseif, M., Hayes, J.L., Basler-Reeder, K., Harry, D.L.,
655 Malazian, A., Dosseto, A., Hartsough, P.C., Hopmans, J.W., 2014. Geophysical constraints
656 on deep weathering and water storage potential in the Southern Sierra Critical Zone Ob-
657 servatory. Earth Surface Processes and Landforms 39, 366–380. doi:10.1002/esp.3502.

658 Holland, T.J.B., 1989. Dependence of entropy on volume for silicate and oxide minerals - A
659 review and a predictive model. American Mineralogist 74, 5–13.

660 Huertas, F.J., Chou, L., Wollast, R., 1998. Mechanism of kaolinite dissolution at room
661 temperature and pressure: Part 1. Surface speciation. Geochimica et Cosmochimica Acta
662 62, 417–431. doi:10.1016/s0016-7037(97)00366-9.

663 Huertas, F.J., Chou, L., Wollast, R., 1999. Mechanism of kaolinite dissolution at room
664 temperature and pressure Part II: Kinetic study. Geochimica et Cosmochimica Acta 63,
665 3261–3275. doi:10.1016/s0016-7037(99)00249-5.

666 Hunsaker, C.T., Johnson, D.W., 2017. Concentration-discharge relationships in headwa-
667 ter streams of the Sierra Nevada, California. Water Resources Research 53, 7869–7884.
668 doi:10.1002/2016wr019693.

669 Jasechko, S., Kirchner, J.W., Welker, J.M., McDonnell, J.J., 2016. Substantial propor-
670 tion of global streamflow less than three months old. Nature Geoscience 9, 126–+.
671 doi:10.1038/ngeo2636.

672 Johnson, J.W., Oelkers, E.H., Helgeson, H.C., 1992. SUPCRT92 - A software package for cal-
673 culating the standard molal thermodynamic properties of minerals, gases, aqueous species,
674 and reactions from 1-bar to 5000-bar and 0-degrees-C to 1000-degrees-C. Computers &
675 Geosciences 18, 899–947. doi:10.1016/0098-3004(92)90029-q.

676 Kurtz, A.C., Derry, L.A., Chadwick, O.A., 2002. Germanium-silicon fractionation
677 in the weathering environment. Geochimica et Cosmochimica Acta 66, 1525–1537.
678 doi:10.1016/s0016-7037(01)00869-9.

679 Kurtz, A.C., Lugolobi, F., Salvucci, G., 2011. Germanium-silicon as a flow path
680 tracer: Application to the Rio Icacos watershed. Water Resources Research 47, 16.
681 doi:10.1029/2010wr009853.

682 Lasaga, A.C., 1981. Rate laws of chemical reactions, in: Lasaga, A.C., Kirkpatrick, R.J.
683 (Eds.), Kinetics of Geochemical Processes. Mineralogical Society of America, Reviews in
684 Mineralogy. volume 8, pp. 1–67.

685 Liu, F.J., Hunsaker, C., Bales, R.C., 2013. Controls of streamflow generation in small

686 catchments across the snow-rain transition in the Southern Sierra Nevada, California.
687 Hydrological Processes 27, 1959–1972. doi:10.1002/hyp.9304.

688 Lugolobi, F., Kurtz, A.C., Derry, L.A., 2010. Germanium-silicon fractionation in a tropi-
689 cal, granitic weathering environment. Geochimica et Cosmochimica Acta 74, 1294–1308.
690 doi:10.1016/j.gca.2009.11.027.

691 Maher, K., Steefel, C.I., DePaolo, D.J., Viani, B.E., 2006. The mineral dissolution
692 rate conundrum: Insights from reactive transport modeling of U isotopes and pore
693 fluid chemistry in marine sediments. Geochimica et Cosmochimica Acta 70, 337–363.
694 doi:10.1016/j.gca.2005.09.001.

695 Maher, K., Steefel, C.I., White, A.F., Stonestrom, D.A., 2009. The role of reaction affin-
696 ity and secondary minerals in regulating chemical weathering rates at the Santa Cruz
697 Soil Chronosequence, California. Geochimica et Cosmochimica Acta 73, 2804–2831.
698 doi:10.1016/j.gca.2009.01.030.

699 Martin, F., Ildefonse, P., Hazemann, J.L., Petit, S., Grauby, O., Decarreau, A., 1996. Ran-
700 dom distribution of Ge and Si in synthetic talc: An EXAFS and FTIR study. European
701 Journal of Mineralogy 8, 289–299. doi:10.1127/ejm/8/2/0289.

702 Martin, F., Petit, S., Decarreau, A., Grauby, O., Hazemann, J.L., Noack, Y., 1992.
703 Experimental-study of Si-Ge tetrahedral solid-solution in Ni-Co-Mg talcs. Thin Solid
704 Films 222, 189–195. doi:10.1016/0040-6090(92)90066-k.

705 Marty, N.C.M., Claret, F., Lassin, A., Tremosa, J., Blanc, P., Made, B., Gif-
706 faut, E., Cochepin, B., Tournassat, C., 2015. A database of dissolution and
707 precipitation rates for clay-rocks minerals. Applied Geochemistry 55, 108–118.
708 doi:10.1016/j.apgeochem.2014.10.012.

709 Medvedev, V.A., Bergman, G.A., Vasiliev, V.P., 1981. Thermal Constants of Materials: A
710 Reference Book, in: Glushko, V.P. (Ed.), The Thermal Constants of Subtances. VINITI,
711 Moscow. volume 10, pp. 1965–82.

712 Metz, V., Ganor, J., 2001. Stirring effect on kaolinite dissolution rate. Geochimica et
713 Cosmochimica Acta 65, 3475–3490. doi:10.1016/s0016-7037(01)00686-x.

714 Mortlock, R.A., Froelich, P.N., 1987. Continental weathering of germanium - Ge/Si
715 in the global river discharge. Geochimica et Cosmochimica Acta 51, 2075–2082.
716 doi:10.1016/0016-7037(87)90257-2.

717 Murnane, R.J., Stallard, R.F., 1990. Germanium and silicon in rivers of the orinoco drainage-
718 basin. Nature 344, 749–752. doi:10.1038/344749a0.

719 Nagy, K.L., Blum, A.E., Lasaga, A.C., 1991. Dissolution and precipitation kinetics of kaoli-
720 nite at 80-degrees-C and pH 3: The dependence on solution saturation state. American
721 Journal of Science 291, 649–686. doi:10.2475/ajs.291.7.649.

722 Opfergelt, S., Cardinal, D., Andre, L., Delvigne, C., Bremond, L., Delvaux, B., 2010.
723 Variations of Delta Si-30 and Ge/Si with weathering and biogenic input in tropical
724 basaltic ash soils under monoculture. Geochimica et Cosmochimica Acta 74, 225–240.
725 doi:10.1016/j.gca.2009.09.025.

726 Pokrovski, G.S., Schott, J., 1998. Thermodynamic properties of aqueous Ge(IV) hydroxide
727 complexes from 25 to 350 degrees C: Implications for the behavior of germanium and the
728 Ge/Si ratio in hydrothermal fluids. Geochimica et Cosmochimica Acta 62, 1631–1642.
729 doi:10.1016/s0016-7037(98)00081-7.

730 Prieto, M., 2009. Thermodynamics of Solid Solution-Aqueous Solution Systems. Thermo-
731 dynamics and Kinetics of Water-Rock Interaction 70, 47–85. doi:10.2138/rmg.2009.70.2.

732 Prieto, M., FernandezGonzalez, A., Putnis, A., FernandezDiaz, L., 1997. Nucleation, growth,
733 and zoning phenomena in crystallizing (Ba,Sr)CO3, Ba(SO4,CrO4), (Ba,Sr)SO4, and
734 (Cd,Ca)CO3 solid solutions from aqueous solutions. Geochimica et Cosmochimica Acta
735 61, 3383–3397. doi:10.1016/s0016-7037(97)00160-9.

736 Prieto, M., Heberling, F., Rodriguez-Galan, R.M., Brandt, F., 2016. Crystalliza-
737 tion behavior of solid solutions from aqueous solutions: An environmental perspec-

tive. Progress in Crystal Growth and Characterization of Materials 62, 29–68. doi:10.1016/j.pcrysgrow.2016.05.001.

Putnis, A., Fernandezdiaz, L., Prieto, M., 1992. Experimentally produced oscillatory zoning in the (Ba, Sr)SO4 solid-solution. Nature 358, 743–745. doi:10.1038/358743a0.

Qi, H.W., Hu, R.Z., Jiang, K., Zhou, T., Liu, Y.F., Xiong, Y.W., 2019. Germanium isotopes and Ge/Si fractionation under extreme tropical weathering of basalts from the Hainan Island, South China. Geochimica et Cosmochimica Acta 253, 249–266. doi:10.1016/j.gca.2019.03.022.

Rademacher, L.K., Clark, J.F., Clow, D.W., Hudson, G.B., 2005. Old groundwater influence on stream hydrochemistry and catchment response times in a small Sierra Nevada catchment: Sagehen Creek, California. Water Resources Research 41, 10. doi:10.1029/2003wr002805.

Safeeq, M., Hunsaker, C.T., 2016. Characterizing runoff and water yield for headwater catchments in the Southern Sierra Nevada. Journal of the American Water Resources Association 52, 1327–1346. doi:10.1111/1752-1688.12457.

Scribner, A.M., Kurtz, A.C., Chadwick, O.A., 2006. Germanium sequestration by soil: Targeting the roles of secondary clays and Fe-oxyhydroxides. Earth and Planetary Science Letters 243, 760–770. doi:10.1016/j.epsl.2006.01.051.

Shtenberg, M.V., Bychinskii, V.A., Koroleva, O.N., Korobatova, N.M., Tupitsyn, A.A., Fomichev, S.V., Krenev, V.A., 2017. Calculation of the formation enthalpies, standard entropies, and standard heat capacities of alkali and alkaline-earth germanates. Russian Journal of Inorganic Chemistry 62, 1464–1468. doi:10.1134/s0036023617110183.

Sprenger, M., Stumpp, C., Weiler, M., Aeschbach, W., Allen, S.T., Benettin, P., Dubbert, M., Hartmann, A., Hrachowitz, M., Kirchner, J.W., McDonnell, J.J., Orlowski, N., Penna, D., Pfahl, S., Rinderer, M., Rodriguez, N., Schmidt, M., Werner, C., 2019. The Demographics of Water: A Review of Water Ages in the Critical Zone. Reviews of Geophysics 57, 800–834. doi:10.1029/2018rg000633.

765 Steefel, C.I., Appelo, C.A.J., Arora, B., Jacques, D., Kalbacher, T., Kolditz, O., Lagneau,
766 V., Lichtner, P.C., Mayer, K.U., Meeussen, J.C.L., Molins, S., Moulton, D., Shao,
767 H., Simunek, J., Spycher, N., Yabusaki, S.B., Yeh, G.T., 2015. Reactive transport
768 codes for subsurface environmental simulation. Computational Geosciences 19, 445–478.
769 doi:10.1007/s10596-014-9443-x.

770 Steefel, C.I., Druhan, J.L., Maher, K., 2014. Modeling coupled chemical and iso-
771 topic equilibration rates, in: Gaillardet, J. (Ed.), Geochemistry of the Earth's
772 Surface Ges-10. volume 10 of *Procedia Earth and Planetary Science*, pp. 208–217.
773 doi:10.1016/j.proeps.2014.08.022.

774 Tardy, Y., Garrels, R.M., 1977. Prediction of Gibbs energies of formation of compounds
775 from elements. 2. Monovalent and divalent metal silicates. Geochimica et Cosmochimica
776 Acta 41, 87–92. doi:10.1016/0016-7037(77)90189-2.

777 Vieillard, P., 1994. Prediction of enthalpy of formation based on refined crystal-structures
778 of multisite compounds. 1. Theories and examples. Geochimica et Cosmochimica Acta 58,
779 4049–4063. doi:10.1016/0016-7037(94)90266-6.

780 Vieillard, P., Tardy, Y., 1988. Estimation of enthalpies of formation of minerals based on
781 their refined crystal-structures. American Journal of Science 288, 997–1040.

782 Wada, S., Wada, K., 1982. Effects of substition of germanium for silicon in imogolite. Clays
783 and Clay Minerals 30, 123–128. doi:10.1346/ccmn.1982.0300206.

784 White, A.F., Brantley, S.L., 2003. The effect of time on the weathering of silicate minerals:
785 why do weathering rates differ in the laboratory and field? Chemical Geology 202, 479–
786 506. doi:10.1016/j.chemgeo.2003.03.001.

787 Yang, L., Steefel, C.I., 2008. Kaolinite dissolution and precipitation kinetics at 22 degrees C
788 and pH 4. Geochimica et Cosmochimica Acta 72, 99–116. doi:10.1016/j.gca.2007.10.011.

789 Zhu, C., Rimstidt, J.D., Zhang, Y.L., Kang, J.T., Schott, J., Yuan, H.L., 2020. Decoupling
790 feldspar dissolution and precipitation rates at near-equilibrium with Si isotope tracers:

Implications for modeling silicate weathering. Geochimica et Cosmochimica Acta 271, 132–153. doi:10.1016/j.gca.2019.12.024.

Zimmer, K., Zhang, Y.L., Lu, P., Chen, Y.Y., Zhang, G.R., Dalkilic, M., Zhu, C., 2016. SUPCRTBL: A revised and extended thermodynamic dataset and software package of SUPCRT92. Computers & Geosciences 90, 97–111. doi:10.1016/j.cageo.2016.02.013.

796 ## Figures

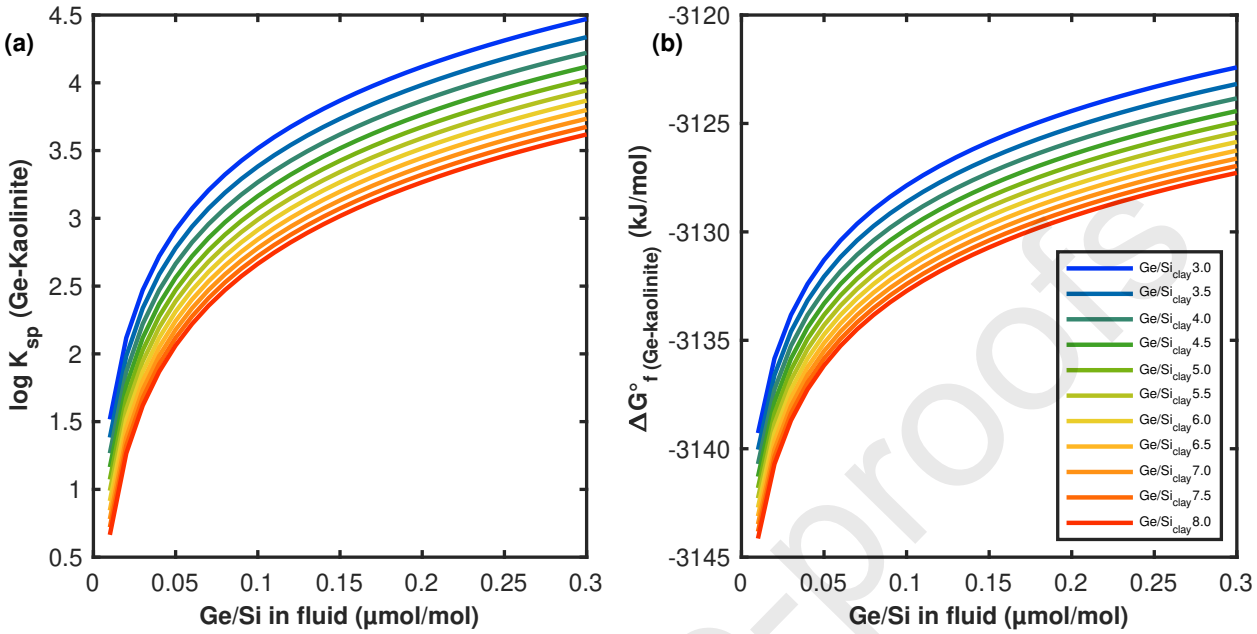

Figure 1: (a) Equilibrium constants as a function of Ge/Si ratios in the fluid in the 0.01-0.3 µmol/mol range. The colored curves show the trajectories for given $(Ge/Si)_{clay}$ ratios. Fractionation between the fluid and the solid is larger as K_{sp} becomes smaller. For example, a $(Ge/Si)_{clay} = 5.5$ and $(Ge/Si)_{fluid} = 0.1$ µmol/mol, imply a $\log(K_{sp})$ for Ge-kaolinite = 3. (b) Calculated Gibbs energy of formation for Ge-kaolinite as a function of $(Ge/Si)_{fluid}$ based in the hydrolysis of Ge-kaolinite. Thermodynamic data for the aqueous species used for this reaction—$Ge(OH)_4$, $Si(OH)_4$ and Al^{3+}—are from the Thermoddem database and references therein (Blanc et al., 2012) (Table S1).

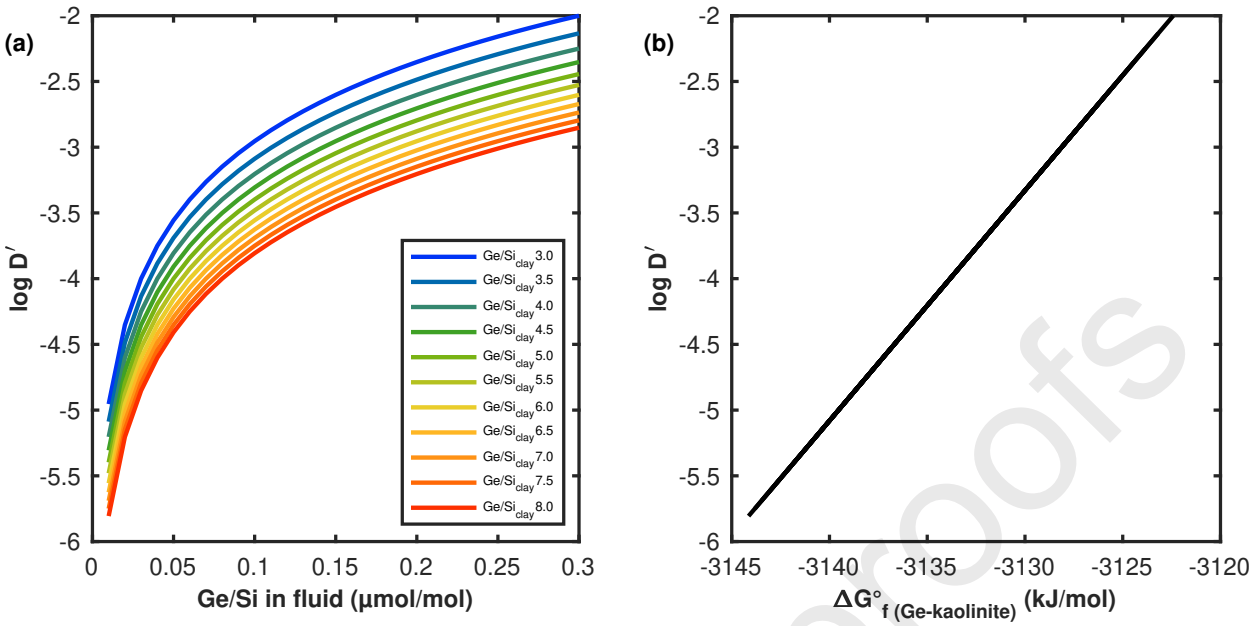

Figure 2: (a) Distribution coefficient D'_{Ge-Si} as a function of $(Ge/Si)_{fluid}$ ratios. The colored curves show the trajectories for given $(Ge/Si)_{clay}$ ratios. (b) Partition coefficient D'_{Ge-Si} as a function of calculated Gibbs energy of formation for Ge-kaolinite.

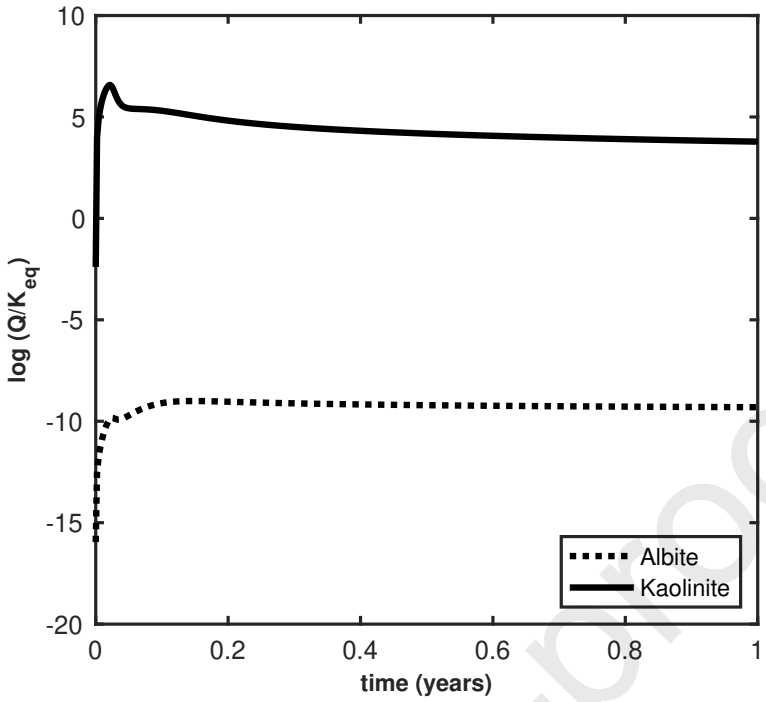

Figure 3: Saturation indexes for albite (dotted-line) and kaolinite (solid-line) as a function of time during the base batch-reactor model of plagioclase dissolution and kaolinite precipitation.

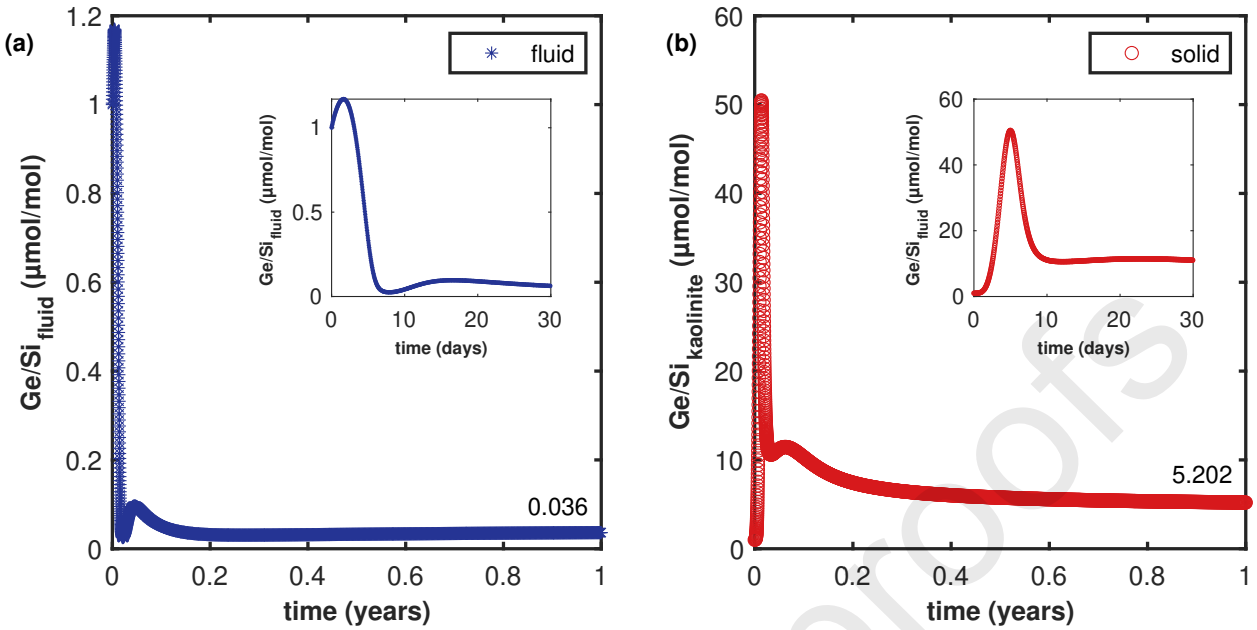

Figure 4: (a) Evolution of Ge/Si ratios in the fluid (µmol/mol) for the batch dissolution-precipitation base model with $D'_{Ge-Si} = 4 \times 10^{-4}$. (b) Evolution of the bulk Ge/Si ratio in the precipitated kaolinite solid solution (µmol/mol). The Ge/Si ratios in the fluid and solid at timestep = 1 year are indicated in the figure. The inserts show the transient behavior during the first 30 days, where the incipient solid has a much higher Ge/Si ratio.

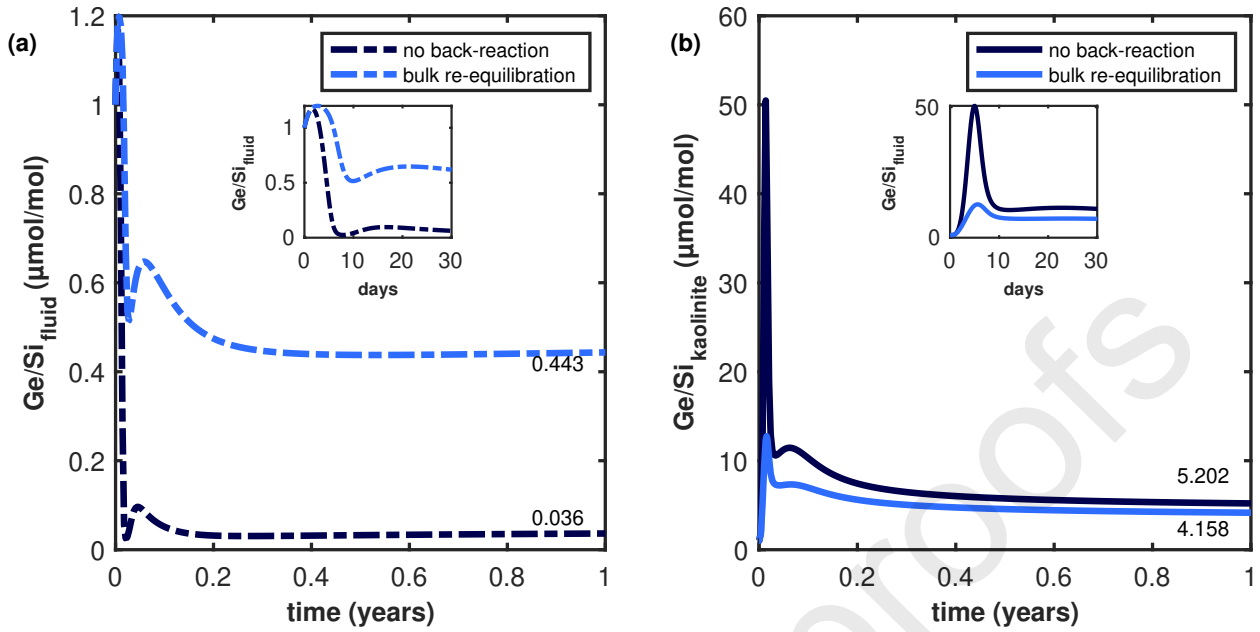

Figure 5: The effect of mineral and fluid re-equilibration on Ge/Si ratios. (a) Evolution of the Ge/Si ratio in the fluid with no back reaction for Equation 11 (dark blue dash-dot) and with re-equilibration with the bulk solid for Equation 8 (light blue dash-dot) for $D'_{Ge-Si} = 4 \times 10^{-4}$. (b) Ge/Si ratios in the solid (solid lines), legend colors is the same as in (a). The Ge/Si ratios in the fluid and solid at timestep = 1 year are indicated in the figure for both cases. Inserts show the first 30 days.

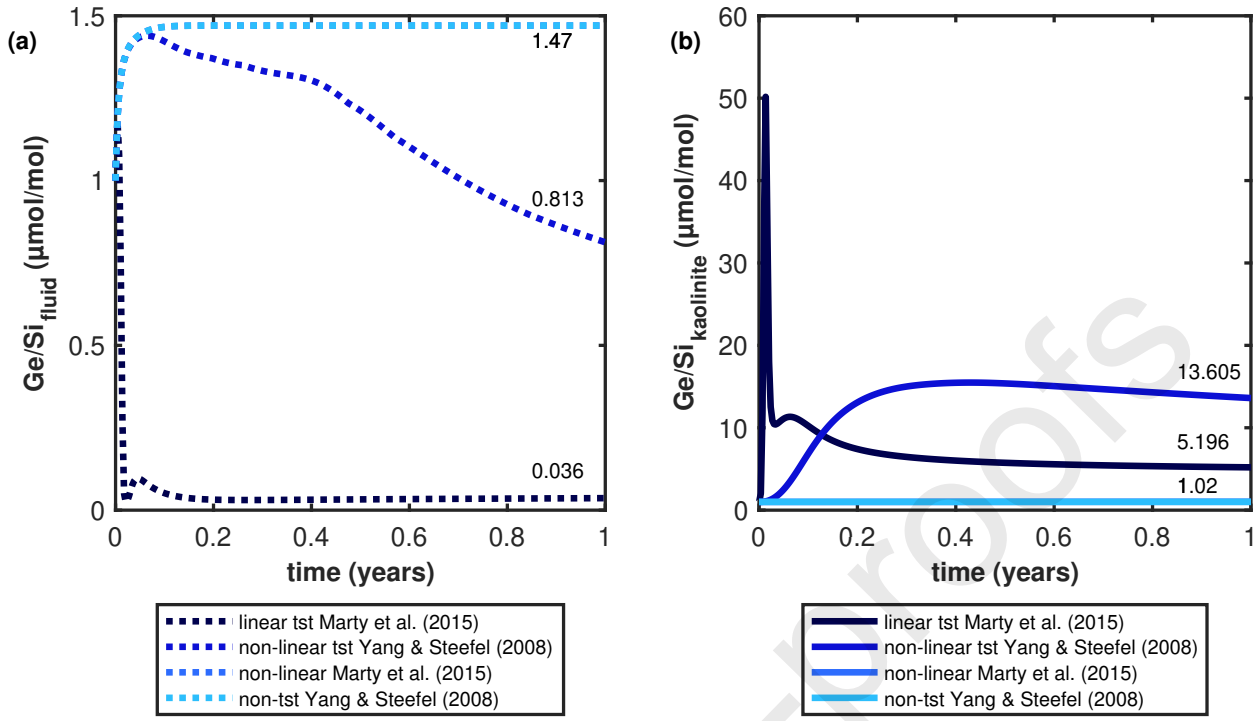

Figure 6: (a) The effect of precipitation rate with a non-linear dependence on the affinity term for TST (Yang and Steefel, 2008; Marty et al., 2015) and non-TST (Yang and Steefel, 2008) in Ge/Si fluid ratios at 1-year timescales (b) Evolution of Ge/Si ratios in the precipitated mineral solid solution for the same rate laws. The Ge/Si ratios in the fluid and solid at time-step = 1 year are indicated in the figure for each rate-law. Note that in (a) the result for the non-linear (Marty et al., 2015) formulation is nearly identical with the non-TST formulation of Yang and Steefel (2008), and so the two curves plot on top of one another, expected because the Marty et al. (2015) is a parametrization of the data used by Nagy et al. (1991) and Yang and Steefel (2008).

Tables

Recommended ΔG_f° and ${}^{Ge}K_{sp}$ values for $Ge_2Al_2O_5(OH)_4$		
ΔG_f°	-3130.40 ±15	(kJ/mol)
$\log({}^{Ge}K_{sp})$ [1]	3.073 ± 1.5	

[1] Aqueous species data Blanc et al. (2012).

Table 1: Recommended thermodynamic properties for $Ge_2Al_2O_5(OH)_4$ from the equilibrium fractionation model. Equilibrium constant is for the reaction 2. The G_f° and ${}^{Ge}K_{sp}$ were calculated assuming an equilibrium fractionation factor $D'_{Ge-Si} = 4 \times 10^{-4}$.

Structural parameters to estimate ΔH_f° and S_f°		
$\Delta_H O^{=} Ge^{4+}_{(aq)}$	-223.52 ± ∼ 0	(kJ/mol)
$\Delta_S O^{=} Ge^{4+}_{(aq)}$	276.59 ± 0.32	(J/mol/K)
Estimated thermodynamic properties for $Ge_2Al_2O_5(OH)_4$		
ΔG_f°	–3094.03 ± 40	(kJ/mol)
ΔH_f°	–3422.46 ± 30	(kJ/mol)
S_f°	201.89 ± 91	(J/mol/K)
$\log(^{Ge}K_{sp})$ [1]	9.30 ± 7.00	

[1] Aqueous species data Blanc et al. (2012). See Table S1 for $GeO_{2(hex)}$ and Ge^{4+} data.

Table 2: Estimated thermodynamic properties for $Ge_2Al_2O_5(OH)_4$ using the parametric model developed by Blanc et al. (2015). Equilibrium constant is for the reaction 2.

Mineral	$\log K_{sp}$	V m^3/m^3	A_{SSA}[1] m^2/g	$\log k_f$ $mol/m^2/s$	n_1	n_2	Rate-law Type	Reference
Albite	2.996 [1]	0.3	0.0091	-11.89	—	—	Linear TST	Marty et al. (2015)
Kaolinite	6.471 [1]1]	10^{-8}	0.64	-13.66	—	—	Linear TST	Marty et al. (2015)
				-12.94	0.5	—	non-linear TST	Yang and Steefel (2008)
				-12.26	1.68	0.06	Non-linear non-TST	Marty et al. (2015)
				-13.47	2.07	-1.00	Non-linear non-TST	Yang and Steefel (2008)
Ge-kaolinite	3.073 [2]	10^{-14}	0.64	-13.96	—	—	Linear TST	Marty et al. (2015)
				-12.94	0.5	—	non-linear TST	Yang and Steefel (2008)
				-12.26	1.68	0.06	Non-linear non-TST	Marty et al. (2015)
				-13.47	2.07	-1.00	Non-linear non-TST	Yang and Steefel (2008)

[1] Blanc et al. (2012). [2] This study.

Table 3: Model parameters for the batch dissolution numerical experiments in CrunchFlow. Equilibrium constants for the hydrolysis of albite (Eq. 1), Si-kaolinite (Eq. 3) and Ge-kaolinite (Eq. 2). Specific surface area (SSA), volume fraction, rate constants and coefficients (Equation 7). Specific surface area (SSA) can be multiplied by molar mass and volume fraction, and divided by the molar volume to obtain A_{bulk} as in Equation 7. The rate constants from Marty et al. (2015) are regressed from experimental data, see references therein. Note that the volume fraction for Kaolinite and Ge-kaolinite is provided to start precipitation with an initial $Ge/Si = 1$ (µmol/mol).